THE IMPORTANCE OF SPECTROSCOPY IN THE 80–800 Å REGION FOR PLASMA DIAGNOSTICS IN THE SOLAR ATMOSPHERE

U. FELDMAN* and G. A. DOSCHEK

E. O. Hulburt Center for Space Research, Naval Research Laboratory, Washington, D.C. 20375, U.S.A.

and

W. E. BEHRING

Laboratory for Astronomy and Solar Physics, Goddard Space Flight Center, Greenbelt, Md 20771, U.S.A.

(Received 7 September, 1978)

Abstract. We discuss the importance of the spectral range from about 80 to 800 Å for determining physical conditions in different regions of the solar atmosphere. We give examples of line ratios that may be used to determine electron densities in quiet Sun regions, active regions, and flares. We discuss the possibility of determining electron temperatures from line ratios in the EUV.

We show that profiles as well as intensities of spectral lines must be obtained for a proper interpretation of the spectra. We give approximate parameters for a solar grazing incidence spectrograph suitable for the study of the 80–800 Å wavelength region.

1. Introduction

The region of the solar spectrum between about 80 and 800 Å has not been thoroughly explored with spectral resolution adequate for the measurement of coronal line profiles. The wavelength range from about 270 to 1350 Å was covered by the normal incidence Harvard spectroheliometers on the fourth and sixth Orbiting Solar Observatories and on *Skylab*, but the spectral resolution was never better than $\simeq$0.8 Å. The slitless spectrographs flown by NRL on rockets and on *Skylab* covered the range from $\simeq$170 to $\simeq$600 Å, but the spatial imaging properties of these instruments preclude good spectral resolution. Grazing incidence spectrographs have been flown on OSO satellites and rockets, but only the instruments flown by Behring *et al.* (1972, 1976) and Cushman *et al.* (1975) had sufficient resolution to record line profiles.

The object of this review is to show that the wavelength region between 80 and 800 Å (the grazing incidence region)† is one of the most important spectral regions for the study of phenomena in the solar atmosphere, from the standpoint of spectral diagnostics. It therefore seems that an effort should be made to fly a high spectral resolution spectrograph or spectrometer on a future space mission, perhaps the Shuttle, that would record spectra in the 80–800 Å region. There is no technological reason why such an instrument could not be built.

* Given as an invited review paper at the EGAS Meeting in Münich, Germany, 11–14 July 1978.

† In this paper, we call the wavelength region 80–800 Å the grazing incidence region even though wavelengths as low as $\simeq$200 Å can be recorded by a normal incidence spectrograph.

Space Science Reviews **22** (1978) 191–212.

In Section 2 we discuss the types of lines that appear in the 80–800 Å range and the expected widths of these lines in different regions of the solar atmosphere. In Section 3 we summarize most of the extensive work that has recently been done on electron density diagnostics in the 80–800 Å range. In Section 4 we discuss the possibility of determining electron temperatures from line ratios in this region. In Section 5 we discuss the importance of having both line intensity and profile information for proper interpretation of spectra. Finally, in Section 6 we discuss a particular spectrograph that covers the 80–800 Å range and that would enable the measurements described in the preceding sections to be carried out.

2. Spectral Lines in the 80–800 Å Region

In the region between 80 and 800 Å there are lines emitted from the chromosphere, the transition zone, and the corona. The main chromospheric lines are the He I and He II resonance lines. The resonance lines of certain transition zone ions appear in this region as well, e.g., O V ($2s^2\,{}^1S_0 - 2s2p\,{}^1P_1$, 629 Å). However, most of the lines that fall below 800 Å belong to coronal ions, i.e., ions formed at temperatures $\geq 8 \times 10^5$ K. Some of these lines are emitted from the quiet and active corona while others appear only during flares. Coronal flare plasma usually spans a temperature

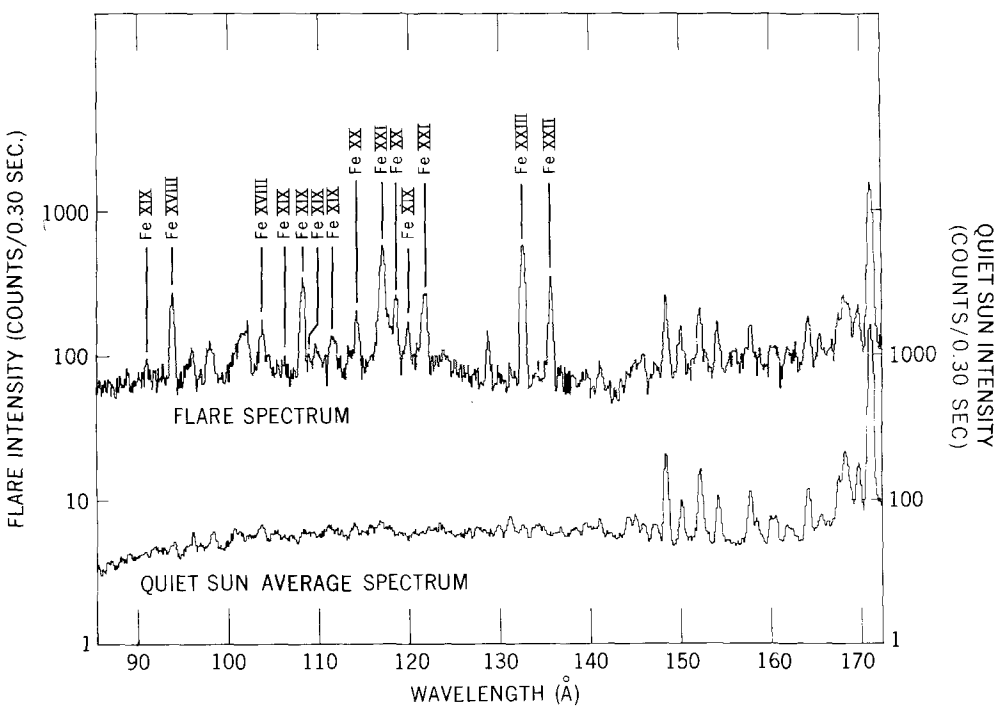

Fig. 1. Average quiet Sun spectrum and flare spectrum recorded by a GSFC spectrometer on OSO-5 (see Kastner *et al.*, 1974).

range between about 10^6 K and a few times 10^7 K. Many of the additional lines that appear at short wavelengths near $\simeq 100$ Å during flares are due to allowed transitions of the type $2s^2 2p^k - 2s2p^{k+1}$, mostly from Fe XVIII through Fe XXIII. The only spectra showing these lines were recorded by the Goddard spectrometer on OSO-V (Kastner *et al.*, 1974, see Figure 1). The two Fe XXIV lines fall at appreciably longer wavelengths than the other lines, around 192 and 255 Å, and are strong lines in NRL slitless spectra of flares recorded on *Skylab* (see Figure 2). Consequently, one can study flare plasmas up to temperatures of about 2×10^7 K in the 80–800 Å region. Usually, the study of such plasmas is only considered in the context of X-ray instrumentation.

Extensive line lists for the grazing incidence region are given by Behring *et al.* (1972, 1976) and Malinovsky and Heroux (1973), for the quiet Sun. Dere (1978) has published a list of flare emission lines down to about 170 Å. For wavelengths below 170 Å, a flare list has been published by Kastner *et al.* (1974). Identifications of most of the flare lines due to highly ionized iron are given in Fawcett and Cowan (1975), Kononov *et al.* (1976) and Feldman (1976).

If thermal broadening alone were responsible for solar line widths, the necessary spectral resolution for resolving line profiles could be calculated from the temperatures at which the lines are formed in ionization equilibrium. It is clear that the widths

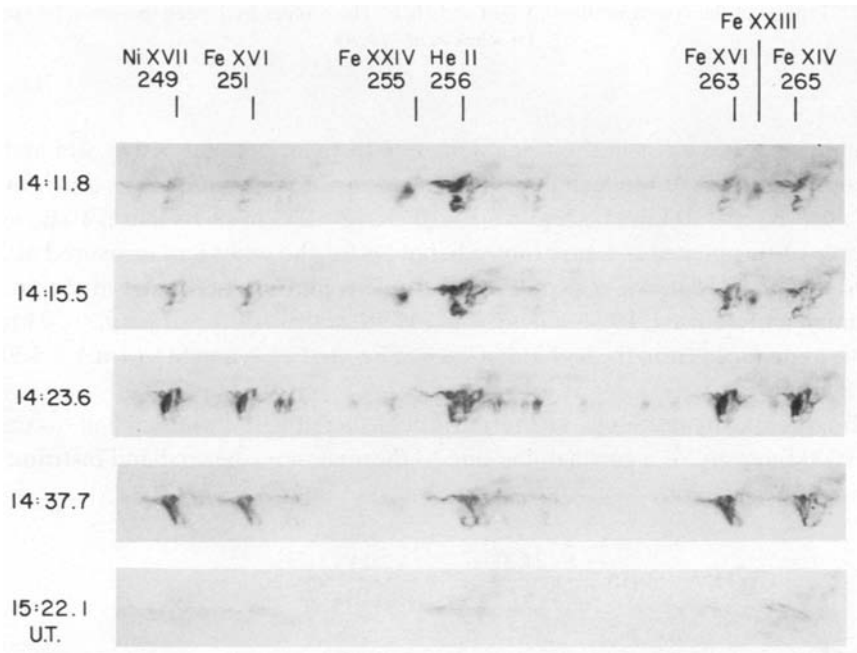

Fig. 2. EUV images of a flare on 15 June 1973 recorded by the NRL slitless spectrograph flown on Skylab. Note the Fe XXIV 255 Å image.

of the coronal and transition zone lines of iron will dictate the spectral resolution, i.e., the He I and He II lines are quite wide and their profiles have been well-determined. From Feldman and Behring (1974), and Doschek *et al.* (1974), the He II 304 Å line is 0.10 Å wide and the He I 584 Å line is about 0.12 Å wide. (The Doschek *et al.* (1974) result for He I has been corrected here for absorption by helium in the Earth's atmosphere.) Figure 3 shows the profiles of these lines. However, we now know that

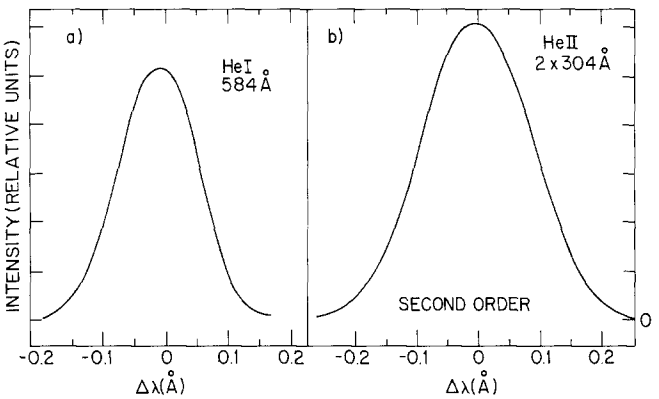

Fig. 3. Profiles of the resonance lines of He I and He II. The profiles have been smoothed by eye (see Doschek *et al.*, 1974).

turbulent motions exist in the transition zone of the quiet and active Sun and the average magnitude of the turbulence is a function of temperature. At a temperature of 2×10^4 K, $\xi\simeq10$ km s^{-1}, and at 2×10^5 K, $\xi\simeq25$ km s^{-1}. Figure 4 shows an example of turbulence vs temperature behavior for the quiet Sun measured at 2–4″ above the limb (Mariska *et al.*, 1978). Turbulent motions also exist in the corona (Feldman and Behring, 1974; Cheng *et al.*, 1978) and are of the order of $\simeq$20 km s^{-1} or less, as deduced from the forbidden lines of Fe XII, Fe XI, and Si VIII at $\lambda > 1000$ Å (see Figure 5).

If broadening by resonance scattering is neglected, the full width at half maximum (FWHM) intensity of a coronal line due to thermal, non-thermal and instrumental broadening is given by

$$\mathrm{FWHM} = 2\sqrt{\ln 2}\,\frac{\lambda}{c}\left(\frac{2kT_i}{M}+\xi^2+\frac{c^2\Delta\lambda_I^2}{4(\ln 2)\lambda^2}\right)^{1/2}, \tag{1}$$

where λ is the wavelength, c is the speed of light, M is the ion mass, T_i is the ion temperature (assumed equal to the electron temperature T_e), ξ is the most probable non-thermal velocity, and $\Delta\lambda_I$ is the instrumental FWHM. Equation (1) assumes a gaussian distribution for both thermal and non-thermal components.

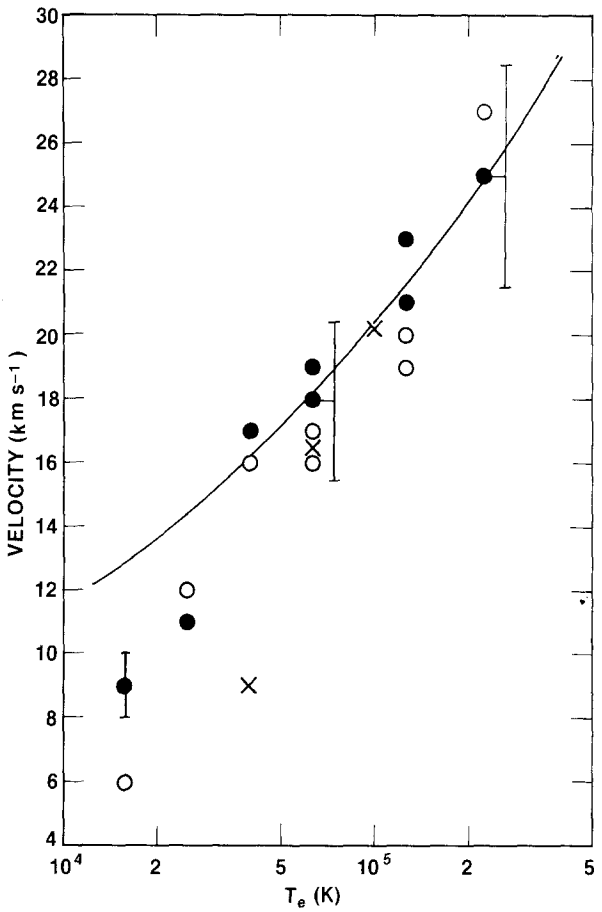

Fig. 4. The nonthermal velocity as a function of electron temperature for transition zone lines. The solid and open circles are from quiet Sun regions observed by NRL and described in Mariska *et al.* (1978). The crosses are from Boland *et al.* (1975). The solid line is the curve predicted assuming that the broadening is caused by an acoustic wave.

Excluding opacity, the broadening to be expected for coronal lines in the grazing incidence region can be estimated from the typical non-thermal velocities deduced by Cheng *et al.* (1978). For the quiet Sun transition zone, line widths can be estimated from the values of ξ given in a number of papers, e.g., Mariska *et al.* (1978). For flares, the FWHM of the forbidden line of Fe XXI at 1354 Å reported by Doschek *et al.* (1975) (Figure 6) provides a guide to the widths of lines of highly ionized flare ions at shorter wavelengths.

The expected line widths of normal coronal lines may be illustrated clearly in graphical form. The FWHM of hypothetical lines of iron and silicon are shown in Figure 7, as a function of λ, T_e, and ξ, as calculated from Equation (1). In order to measure a profile adequately, it is necessary that the instrumental FWHM ($\Delta\lambda_I$) be no wider than about $\frac{1}{3}$ of the true line width. Thus, if $\Delta\lambda_I = 0.02$ Å at 200 Å, adequate resolution will be achieved for most lines.

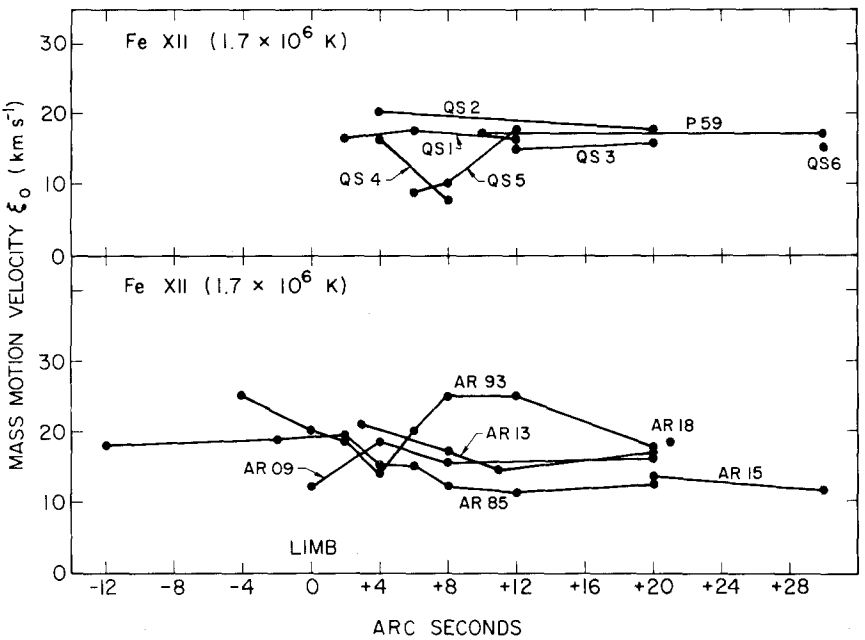

Fig. 5. Nonthermal velocities from Fe XII forbidden line profiles at different heights above the white light limb, QS = quiet Sun, AR = active region, P = prominence (see Cheng *et al.*, 1978).

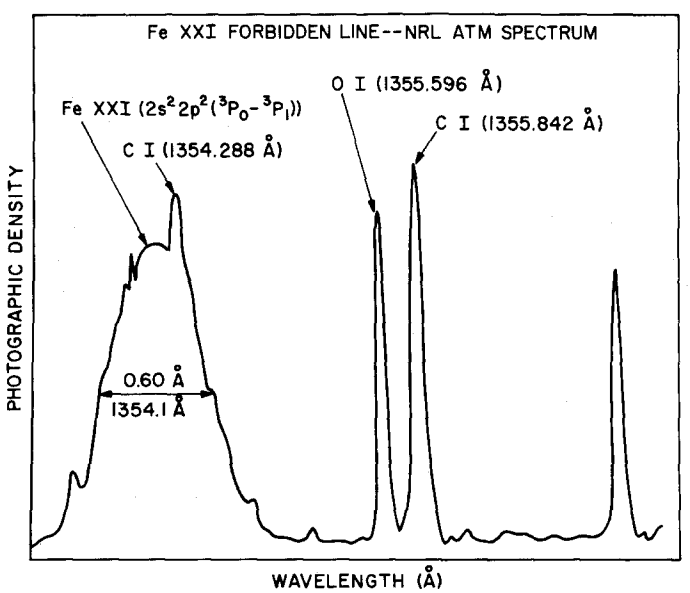

Fig. 6. Flare profile of the Fe XXI forbidden line at 1354 Å (see Doschek *et al.*, 1975).

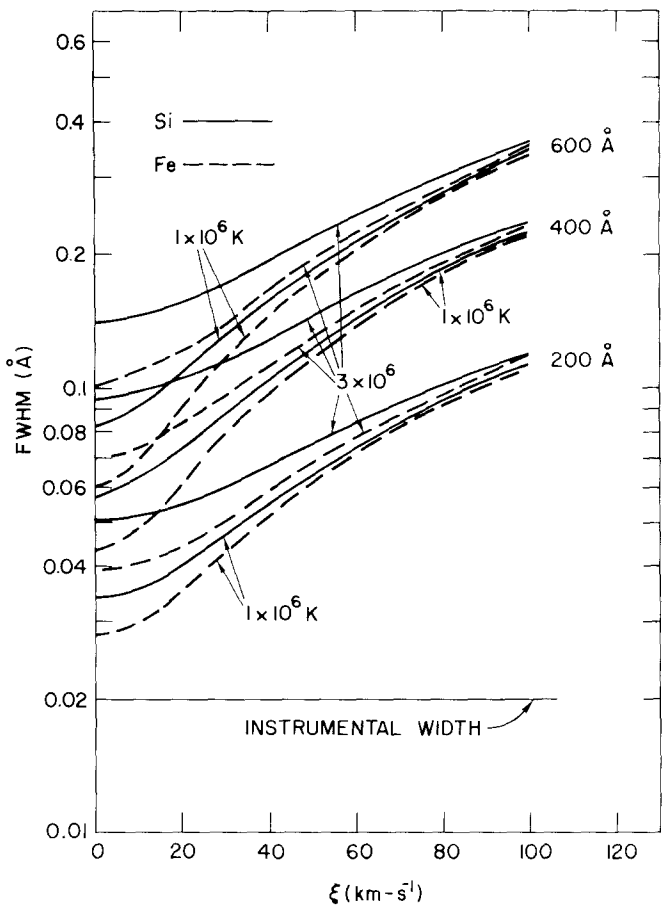

Fig. 7. The FWHM of hypothetical lines of iron and silicon as a function of temperature, wavelength, and nonthermal mass motion. The instrumental width is assumed to be 0.02 Å.

3. Density Diagnostics

There are basically two types of coronal lines in the XUV region – those that arise from 'allowed' transitions, and those that arise from intersystem and forbidden transitions. We define the allowed transitions as those transitions that have very large spontaneous decay rates compared to the rates at which the upper levels of the transitions are populated or depopulated by collisions with electrons and protons. (Photo-excitation is not generally important in the corona compared with collisional processes, although in some instances it must be considered.) The non-allowed transitions arise from metastable levels, e.g., Ne VII ($2s2p\,^3P_1 \rightarrow 2s^2\,^1S_0$). Note that certain transitions forbidden by electric dipole emission, i.e., forbidden lines, might be considered allowed transitions under our definition, as long as the decay rates are much greater than collisional rates. An example is S X ($2p^3\,^2P_{3/2} \rightarrow 2p^3\,^4S_{3/2}$) for $N_e \lesssim 10^9$ cm^{-3}.

Because of these two distinct types of transitions, the intensity ratios of certain spectral lines depend primarily on electron density, and only weakly on other physical parameters. The basis of the method is well-known, dating back to the interpretation of the relative O II line intensities in gaseous nebulae (Aller *et al.*, 1949). Examples of these methods as applied to coronal flare plasmas can be found in Doschek *et al.* (1977a) for Ca XVII, in Feldman *et al.* (1978b) for Fe IX, in Mason *et al.* (1978) for Fe XXI, and in Dere *et al.* (1978) for a number of ions of different isoelectronic sequences that produce lines in the grazing incidence spectral region. The point is that once the collisional excitation rates for populating the excited levels of a particular ion are known, a solution of the statistical equilibrium equations gives the intensity ratios of different pairs of lines as a function of electron density. The density sensitivity arises because the ratio of the population of 'allowed' and metastable levels depends on the electron density. Figure 8 shows the 241.730 and 244.911 Å lines of Fe IX as they appear in the quiet corona, late in the 15 June 1973 flare and during the 21 January 1974 flare.

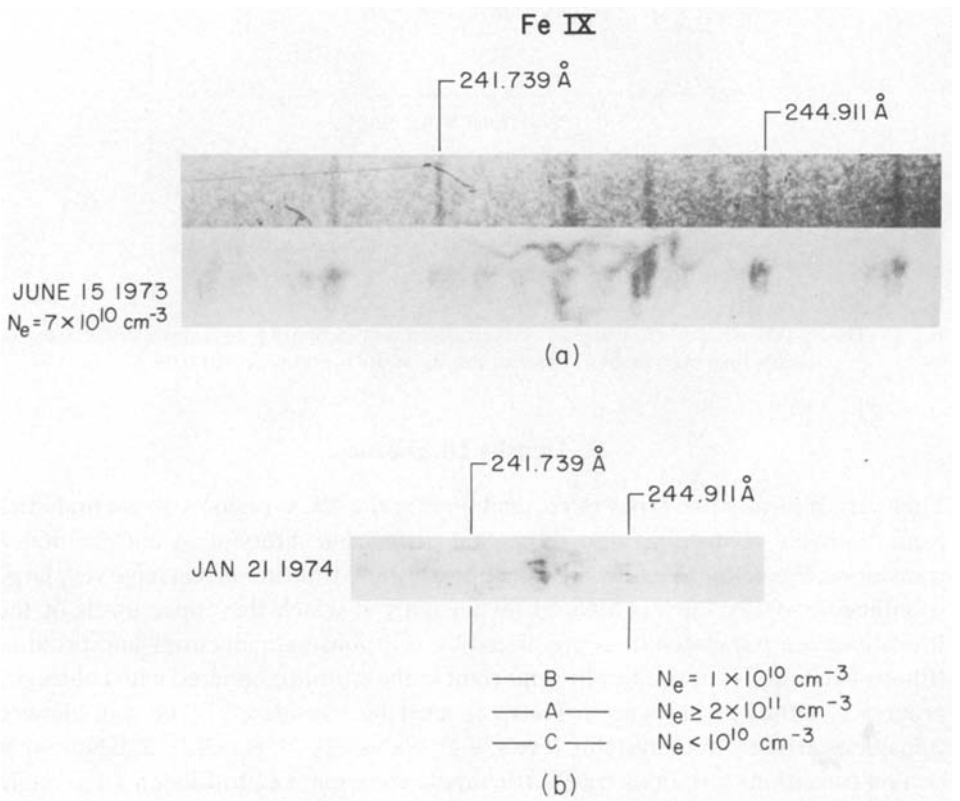

Fig. 8. Behavior of the Fe IX 241.7 Å/244.9 Å ratio in the quiet Sun and in flares and active regions. The slit spectrum is a full disk quiet Sun observation obtained by Behring *et al.* (1976). The slitless spectra were recorded by the NRL instrument on *Skylab*. The theoretical behavior of the Fe IX ratio as a function of electron density is shown in Figure 10 (curve 1). (See Feldman *et al.*, 1978b.)

A systematic study of density sensitive line ratios applicable to different solar regions has been undertaken by a number of investigators (e.g., H. E. Mason, A. K. Bhatia, D. R. Flower, and H. Nussbaumer). These investigators have calculated atomic data for many of the ions that are appreciably abundant in the solar corona. Dere *et al.* (1978) have recently applied the diagnostics that are available in the 170–600 Å region to the flare spectroheliograms recorded by the NRL slitless spectrograph flown on *Skylab*.

The atomic data, as well as line intensity ratios, are available from a number of sources. Some of the atomic data for the B I sequence was supplied to us by Flower (1978), and some was published by Mason and Storey (1978) and Dere *et al.* (1978). The last two references give atomic data and line intensity ratios for Ar XIV, Ca XV, and Fe XXII. Data for the N I and C I sequences were supplied to us in advance of publication by Mason (1978) and Bhatia (1978). These data, including line intensity ratios, are published by Mason and Bhatia (1978), Dere *et al.* (1978), Mason *et al.* (1978), and Bhatia and Mason (1979). The data for Fe XX were calculated by Bhatia and Mason and are not yet published. The atomic data for iron ions are already published i.e., Fe IX (Flower 1977a), Fe X (Mason 1975, Nussbaumer 1976, Mason and Nussbaumer 1977), Fe XI (Mason 1975, Mason and Nussbaumer 1977), Fe XII (Flower 1977b), Fe XIII (Flower and Nussbaumer 1974), Fe XIV (Blaha 1971, Mason 1975) and Fe XV (Bely and Blaha 1968, Dere *et al.* 1977). Useful line ratios for most of the iron lines are given in Dere *et al.* (1978). As yet there appear to be no calculations for the O I sequence except for Ca XIII (Mason, 1975) and Fe XIX (Nussbaumer 1978). We have extrapolated and interpolated results for the Be I sequence from the atomic data given in Gabriel and Jordan (1972). Lines of the Li I sequence are not useful as density diagnostics at solar densities.

Using the above references we have selected a group of density sensitive lines that are applicable to a wide range of density conditions in the corona. Line ratios were calculated for ions of the Be I, B I, C I and N I sequences using a computer program for solving the equations of statistical equilibrium. As mentioned, line ratios for ions of the B I, C I and N I sequences, and for many of the iron ions, are also given in the above references. Ionization equilibrium is assumed in these calculations, and in the following discussions. The photospheric radiation field was included; proton excitation between fine structure levels was not included. We do not believe that the omission of the proton rates will affect the results in a major way. Much of this work appears in the above cited papers.

The selected line ratios are given in Tables I, II, III, and IV, with the approximate ranges for density sensitivity and the wavelengths of the lines. The results for lines within the $n = 3$ configuration of iron ions, and the results for the C I sequence, are shown graphically in Figures 9 and 10. We have used the same line ratios for the C I sequence that were used by Dere *et al.* (1978). These authors also included proton excitation in their calculations.

Because of the ordering of the levels in the C I sequence, it is the best overall sequence for obtaining density sensitive ratios. From Figure 9, density sensitive line ratios can be found that span the density range from 10^8 cm^{-3} to 10^{13} cm^{-3}.

TABLE I

Line ratios in the Be I isoelectronic sequence between the configurations $2s2p$ and $2p^2$ sensitive to densities of 10^{10}–10^{13} electrons cm^{-3}

Ion	Transitions	Wavelengths (Å)	Electron densities (cm^{-3})
Ne VII	$\frac{^3P_1-{}^3P_0}{^3P_0-{}^3P_1}$	$\frac{562.992}{559.947}$	10^{11}–10^{13}
Mg IX	$\frac{^3P_1-{}^3P_0}{^3P_0-{}^3P_1}$	$\frac{445.97}{441.20}$	10^{12}–10^{13}

TABLE II

Line ratios in the B I isoelectronic sequence between the configurations $2s^22p$ and $2s2p^2$ sensitive to densities of 10^9–10^{13} electrons cm^{-3}

Ion	Transitions	Wavelengths (Å)	Electron densities[a] (cm^{-3})
Si X	$\frac{^2P^\circ_{3/2}-{}^2D_{5/2}}{^2P^\circ_{1/2}-{}^2D_{3/2}}$	$\frac{356.038(B)}{347.402(B)}$	10^8–10^{10}
S XII	$\frac{^2P^\circ_{3/2}-{}^2D_{5/2}}{^2P^\circ_{1/2}-{}^2D_{3/2}}$	$\frac{299.536}{288.416}$	10^8–10^{11}
Ar XIV	$\frac{^2P^\circ_{3/2}-{}^2D_{5/2}}{^2P^\circ_{1/2}-{}^2D_{3/2}}$	$\frac{257.368}{243.79}$	10^9–10^{12}
Ca XVI	$\frac{^2P^\circ_{3/2}-{}^2D_{5/2}}{^2P^\circ_{1/2}-{}^2D_{3/2}}$	$\frac{224.54(K1)}{208.57(K1)}$	10^{10}–10^{12}
Fe XXII	$\frac{^2P^\circ_{3/2}-{}^2D_{5/2}}{^2P^\circ_{1/2}-{}^2D_{3/2}}$	$\frac{155.87(K2)}{135.78(K2)}$	10^{12}–10^{14}

[a] The density ranges for Ar XIV, Ca XVI, and Fe XXII were taken from Mason and Storey (1978) and Dere *et al.* (1978).
K1 Kononov *et al.* (1975).
K2 Kononov *et al.* (1976).
B Behring *et al.* (1976).

We may obtain an idea of which ions are best for different solar regions by considering some of the published results concerning densities in the Sun using line ratio techniques. Flare densities have been obtained by Doschek *et al.* (1977a), Feldman *et al.* (1978b), Mason *et al.* (1978) and Dere *et al.* (1978). These results indicate that in coronal flare loops densities on the order of at least 10^{11} to 10^{12} cm^{-3} are achieved at temperatures on the order of 10^6–10^7 K. From Figures 9 and 10 and the tables it is seen that the ions Ne VII, Mg IX, Fe IX, Ca XV, Ca XVI, Ca XVII, and Fe XXI provide the useful diagnostics for flares at these densities. Quiet Sun and active region coronal densities have been derived from an analysis of forbidden line ratios by Feldman *et al.* (1978a). They derived densities of about 10^9 cm^{-3} for the temperature of formation of S X, i.e., 1.3×10^6 K. From the tables and figures it can

TABLE III

Line ratios between the C I $2s^2 2p^2$ and $2s2p^3$ configurations sensitive to densities of 10^8–10^{13} electrons cm^{-3}

Ion		Transitions	Wavelengths (Å)	Electron densities (cm^{-3})
Mg VII[a]	(1)	$\frac{^1D_2 - {}^1D_2^\circ}{^3P_1 - {}^3S_1^\circ}$	$\frac{319.016}{277.042}$	1×10^8–1×10^{10}
Si IX[a]	(2)	$\frac{^1D_2 - {}^1D_2^\circ}{^3P_1 - {}^3P_2^\circ}$	$\frac{258.080(B)}{292.80(B)}$	4×10^8–1×10^{11}
S XI[a]	(3)	$\frac{^1D_2 - {}^1D_2^\circ}{^3P_0 - {}^3S_1^\circ}$	$\frac{215.97}{186.84(B)}$	2×10^9–1×10^{12}
	(4)	$\frac{^3P_2 - {}^3D_3^\circ}{^3P_o - {}^3D_1^\circ}$	$\frac{291.59}{281.416}$	1×10^8–1×10^{10}
Ar XIII[b]	(5)	$\frac{^1D_2 - {}^1D_2^\circ}{^3P_0 - {}^3P_1^\circ}$	$\frac{184.90}{201.69}$	4×10^9–3×10^{12}
	(6)	$\frac{^3P_2 - {}^3D_3^\circ}{^3P_0 - {}^3D_1^\circ}$	$\frac{248.665}{236.267}$	3×10^8–1×10^{11}
	(7)	$\frac{^3P_1 - {}^3D_2^\circ}{^3P_0 - {}^3D_1^\circ}$	$\frac{242.229}{236.267}$	4×10^8–4×10^{10}
Ca XV[b]	(8)	$\frac{^1D_2 - {}^1D_2^\circ}{^3P_0 - {}^3P_1^\circ}$	$\frac{161.00}{171.57}$	1×10^{11}–1×10^{13}
	(9)	$\frac{^3P_2 - {}^3D_3^\circ}{^3P_0 - {}^3D_1^\circ}$	$\frac{215.37}{200.95}$	3×10^{10}–1×10^{13}
	(10)	$\frac{^3P_1 - {}^3D_2^\circ}{^3P_0 - {}^3D_1^\circ}$	$\frac{208.71}{200.95}$	3×10^{10}–1×10^{13}
Fe XXI[c]	(11)	$\frac{^3P_1 - {}^3D_2^\circ}{^3P_0 - {}^3D_1^\circ}$	$\frac{142.14(K2)}{128.73(K2)}$	1×10^{11}–1×10^{13}

K2 Kononov *et al.* (1976). [a] See Mason and Bhatia (1978).
B Behring *et al.* (1976). [b] See Dere *et al.* (1978).
[c] See Mason *et al.* (1978).

be seen that the ions Si IX, S XI, Ar XII, Fe XI, and Fe XIII provide the best diagnostics for this density range. Above 10^{10} cm^{-3}, none of the iron ions is useful except Fe IX, which becomes an excellent diagnostic.

4. Temperature Determinations in the 80–800 Å Region

In ionization equilibrium most of the transition zone and coronal ions are formed primarily over a narrow temperature range (Jordan, 1969). Exceptions are ions with closed shells, and lithiumlike and sodiumlike ions. Therefore, if ionization equilibrium is valid, it is not necessary to determine temperature except for these ions which are abundant over relatively large temperature ranges. The temperatures of most of the lines are in a sense defined by the ionization equilibrium fractional abundance curves, folded into the appropriate excitation rates.

TABLE IV

A list of iron line ratios from the $3s^2 3p^k - 3s3p^{k+1}$ and $3s^2 3p^k - 3s^2 3p^{k-1} 3d$ configurations sensitive to densities of 10^9–10^{13} electrons cm^{-3}

Ion		Transitions	Wavelengths (Å)	Electron densities (cm^{-3})
Fe IX	(1)	$\frac{3p^6\,{}^1S_0 - 3p^5 3d\,{}^3P_2^\circ}{3p^6\,{}^1S_0 - 3p^5 3d\,{}^3P_1^\circ}$	$\frac{241.739}{244.911}$	10^9–10^{12}
Fe XI	(2)	$\frac{3p^4\,{}^1D_2 - 3p^3 3d\,{}^1D_2^\circ}{3p^4\,{}^3P_2 - 3p^3 3d\,{}^3P_2^\circ}$	$\frac{184.793}{188.219}$	10^9–10^{11}
	(3)	$\frac{3p^4\,{}^1D_2 - 3p^3 3d\,{}^1F_3^\circ}{3p^4\,{}^3P_2 - 3p^3 3d\,{}^3P_2^\circ}$	$\frac{179.75}{188.216}$	10^9–10^{11}
Fe XIII	(4)	$\frac{3s^2 3p^2\,{}^1D_2^\circ - 3s3p^3\,{}^1P_1}{3s^2 3p^2\,{}^3P_0^\circ - 3s^2 3p3d\,{}^3P_1}$	$\frac{256.42}{202.06}$	10^9–10^{11}
	(5)	$\frac{3p^2\,{}^3P_2^\circ - 3p3d\,{}^3P_2}{3p^2\,{}^3P_0^\circ - 3p3d\,{}^3P_1}$	$\frac{213.80}{202.06}$	10^9–10^{10}
	(6)	$\frac{3p^2\,{}^1D_2^\circ - 3p3d\,{}^1D_2}{3p^2\,{}^3P_0^\circ - 3p3d\,{}^3P_1}$	$\frac{221.89}{202.06}$	10^9–10^{11}
	(7)	$\frac{3p^2\,{}^3D_2^\circ - 3p3d\,{}^1F_3}{3p^2\,{}^3P_0 - 3p3d\,{}^3P_1}$	$\frac{196.525}{202.06}$	10^9–10^{11}
	(8)	$\frac{3s3p\,{}^3P_2^\circ - 3p^2\,{}^3D_3}{3s3p\,{}^1P_1^\circ - 3p^2\,{}^1D_2}$	$\frac{233.857}{243.790}$	10^9–3×10^{10}

Nevertheless, it has been suggested by many investigators that the ratios of certain line pairs in the grazing incidence region can be used to determine electron temperatures, because of the different Boltzmann factors, $\exp(-\Delta E/kT_e)$, of the two lines. That is, one line is chosen such that the Boltzmann factor is near unity, e.g., a transition of the type, $2s^2 2p^k - 2s2p^{k+1}$. Another line is chosen for which the Boltzmann factor is much smaller than unity, e.g., transitions of the type, $2s^2 2p^k - 2s2p^k 3p$ or $2s^2 2p^k - 2s^2 2p^{k-1} 3s$, $3d$. We show that, if ionization equilibrium is valid, the above method is not a practical temperature diagnostic.

The point is illustrated most clearly by considering a hypothetical three level ion, such that the energy required to excite the third level, ΔE_{13}, is much larger than is required to excite the second level, ΔE_{12}. All excitations are considered to occur from level 1, the ground state, i.e., the coronal approximation is assumed and the populations of levels 2 and 3 are regarded as negligible compared to the population of level 1. We now consider the contributions to the intensities of the two lines with wavelengths λ_{12} and λ_{13}, from two temperature regions. One region is assumed to be at an average temperature T_M where line λ_{12} is emitted with maximum efficiency in ionization equilibrium. The other region is at an average temperature T, that can be regarded as either much lower or much higher than T_M. In reality, a continuous distribution of temperature occurs in the solar atmosphere. Along any given line of sight it is difficult to isolate a structure at a temperature T such that no region at a temperature T_M would be within the field of view. Thus, our two region idealization

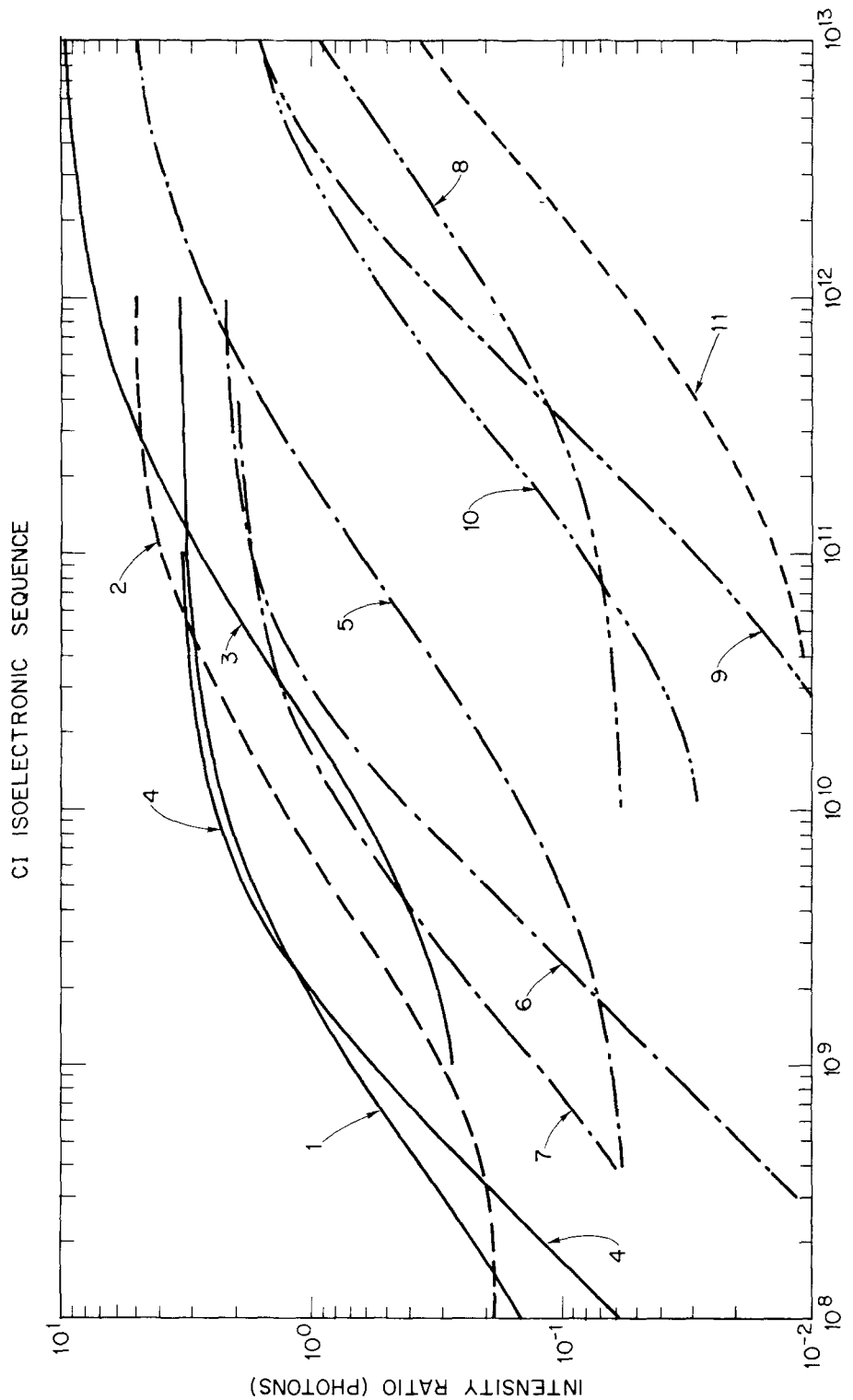

Fig. 9. Density sensitive line ratios in the C I isoelectronic sequence. The numbers refer to the numbers in parentheses in Table III. See Mason and Bhatia (1978) and Dere *et al.* (1978).

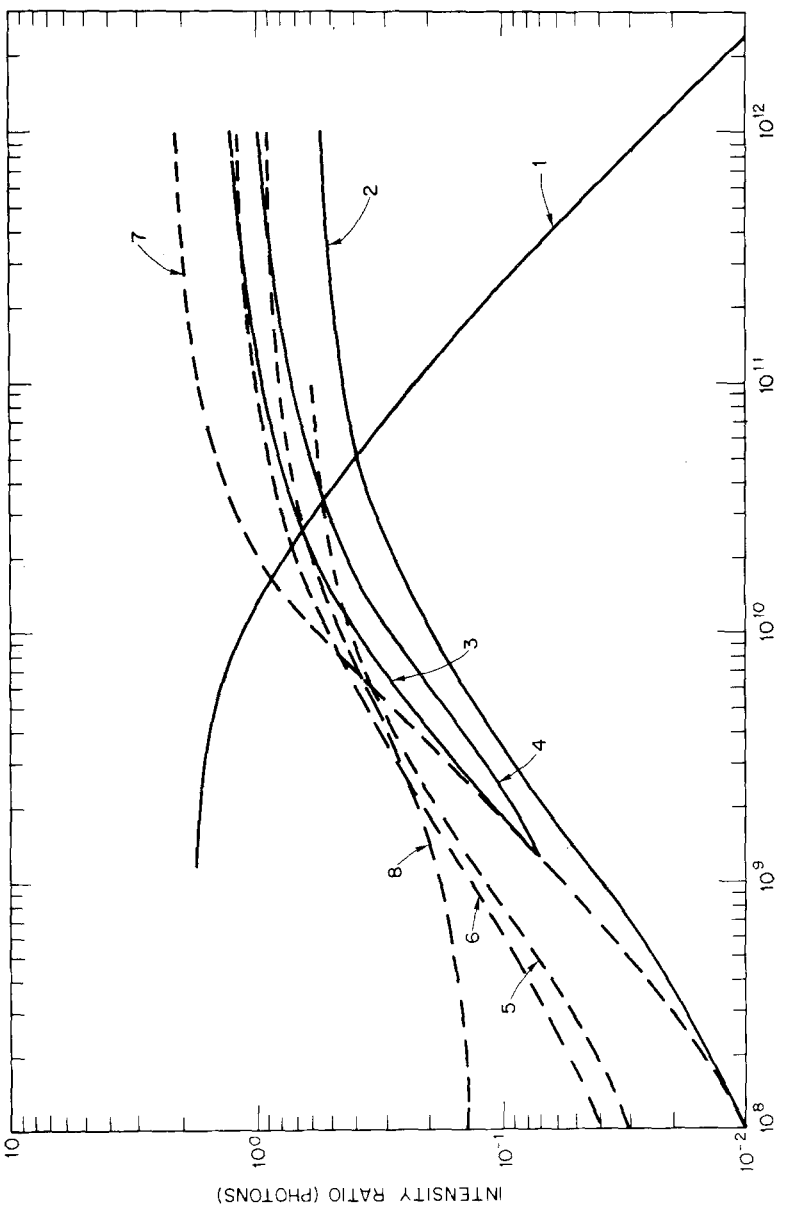

Fig. 10. Density sensitive line ratios of iron ions. The numbers refer to the numbers in parentheses in Table IV. See Dere *et al.* (1978) and Feldman *et al.* (1978b).

has a practical observational basis, and is sufficiently simple to permit a straightforward analysis.

The intensity ratio R of the two lines is given by,

$$R = \frac{\Delta E_{12} \int_{T_M} n_2 A_{21} \, dV + \int_T n_2 A_{21} \, dV}{\Delta E_{13} \int_{T_M} n_3 A_{31} \, dV + \int_T n_3 A_{31} \, dV} \equiv \frac{\Delta E_{12}}{\Delta E_{13}} \frac{[N_2(T_M) + N_2(T)] A_{21}}{[N_3(T_M) + N_3(T)] A_{31}}, \tag{2}$$

where A_{ij} are spontaneous decay rates and n_i are populations of the upper levels. For only one region in ionization equilibrium, the intensity ratio R_0 would be

$$R_0 = \frac{\Delta E_{12}}{\Delta E_{13}} \frac{N_2(T_M)}{N_3(T_M)} \frac{A_{21}}{A_{31}}. \tag{3}$$

The ratio $\alpha = R/R_0$ thus measures the percent change in the line ratio R from its equilibrium ratio R_0. We show that the emission measure of the region at temperature T must be much greater than the emission measure at temperature T_M to change α by even a small amount. Thus, we can only expect to observe appreciable variations in α in the rare situations where a structure with an unusual temperature distribution can be instrumentally isolated from background or foreground radiation.

The ratio α can be written as,

$$\alpha = \left[1 + \frac{N_2(T)}{N_2(T_M)}\right] \Big/ \left[1 + \frac{N_3(T)}{N_3(T_M)}\right]. \tag{4}$$

The functions $N_i(T)$ can be expressed as,

$$N_i(T) \equiv \int_T n_i \, dV = \int_T n_I C_{1i} N_e \, dV, \tag{5}$$

where n_I is the ion population and is equal to,

$$n_I = \frac{n_I}{n_E} \frac{n_E}{n_H} \frac{n_H}{N_e} N_e, \tag{6}$$

where n_E is the element population, $n_E/n_H \equiv A_H$ is the element abundance and $n_I/n_E \equiv F(T)$ is the fractional ion abundance determined from curves such as given in Jordan (1969). In the transition zone and corona, $n_H/N_e \cong 0.8$. The excitation rates $C_{ij}(\text{cm}^3 \text{ s}^{-1})$ can be evaluated in the van Regemorter (1962) approximation, i.e.,

$$C_{1i} = \frac{2.7 \times 10^{-15} \langle \bar{g}_{1i} \rangle f_{1i}}{T^{1/2} \Delta E_{1i}} \exp(-\Delta E_{1i}/kT), \tag{7}$$

where $\langle \bar{g}_{1i} \rangle$ is the Gaunt factor and f_{1i} is the absorption oscillator strength. The integral in Equation (5) can be written as,

$$N_i(T) = 0.8 A_H F(T) C_{1i}(T) \int_T N_e^2 \, dV. \tag{8}$$

Therefore α can be written as,

$$\alpha = \frac{1+\dfrac{\langle \bar{g}_{12}\rangle_T}{\langle \bar{g}_{12}\rangle_{T_M}}\left(\dfrac{T_M}{T}\right)^{1/2}\dfrac{F(T)}{F(T_M)}\exp\left[\dfrac{\Delta E_{12}}{k}\left(\dfrac{1}{T_M}-\dfrac{1}{T}\right)\right]\dfrac{\int_T N_e^2\,\mathrm{d}V}{\int_{T_M} N_e^2\,\mathrm{d}V}}{1+\dfrac{\langle \bar{g}_{13}\rangle_T}{\langle \bar{g}_{13}\rangle_{T_M}}\left(\dfrac{T_M}{T}\right)^{1/2}\dfrac{F(T)}{F(T_M)}\exp\left[\dfrac{\Delta E_{13}}{k}\left(\dfrac{1}{T_M}-\dfrac{1}{T}\right)\right]\dfrac{\int_T N_e^2\,\mathrm{d}V}{\int_{T_M} N_e^2\,\mathrm{d}V}}. \tag{9}$$

By defining the ratio of emission measures as,

$$\beta \equiv \frac{\int_T N_e^2\,\mathrm{d}V}{\int_{T_M} N_e^2\,\mathrm{d}V}, \tag{10}$$

We may rewrite Equation (9) as,

$$\beta = \frac{1-\alpha}{\left(\dfrac{T_M}{T}\right)^{1/2}\dfrac{F(T)}{F(T_M)}\left[\alpha\dfrac{\langle \bar{g}_{13}\rangle_T}{\langle \bar{g}_{13}\rangle_{T_M}}\exp\left[-\dfrac{\Delta E_{13}}{k}\left(\dfrac{1}{T}-\dfrac{1}{T_M}\right)\right]-\dfrac{\langle \bar{g}_{12}\rangle_T}{\langle \bar{g}_{12}\rangle_{T_M}}\exp\left[-\dfrac{\Delta E_{12}}{k}\left(\dfrac{1}{T}-\dfrac{1}{T_M}\right)\right]\right]}. \tag{11}$$

The implications of Equation (11) are best appreciated by considering some examples. Two line pairs that have been suggested as temperature diagnostics are O V 172.17 Å, 629.74 Å, and Si XI 43.74 Å and 303.32 Å. We may determine β as a function of α for two values of T for each line pair, i.e., $0.5T_M$ and $2.0T_M$. The results are given in Table V.

Consider the results for O V first. The ratio β of emission measures of the two regions must be greater than an order of magnitude in order to observe even a factor

TABLE V

α, β parameters

Line pair	T/T_M	α	β
O V (λ629.7/λ172.2)	0.5	1.1	2.6
	0.5	1.5	13
	0.5	2.0	28
	0.5	15.8	∞
O V (λ629.7/λ172.2)	2.0	0.9	1.6
	2.0	0.67	8
	2.0	0.5	21
	2.0	0.252	∞
Si XI (λ303.3/λ43.7)	0.5	1.1	42
	0.5	1.5	231
	0.5	2.0	524
	0.5	5.82	∞
Si XI (λ303.3/λ43.7)	2.0	0.9	3.2
	2.0	0.67	20
	2.0	0.5	92
	2.0	0.416	∞

of two change in α. Thus, the region must be very well isolated from foreground or background equilibrium plasma. The situation is even worse for Si XI. β must be $\simeq 100$ and $\simeq 500$ to observe changes in α of a factor of two.

5. The Value of Line Profiles in the 80–800 Å Region

We have already noted in Section 2 that transition zone and coronal lines are appreciably broadened by non-thermal motions. For transition zone lines, the non-thermal broadening is the dominant contribution to the line width, while for coronal lines the thermal and non-thermal broadening are comparable.

The nonthermal motions in regions of activity have been studied by Doschek *et al.* (1977b), Feldman *et al.* (1977), and by Doschek and Feldman (1978). They analyzed transition zone line profiles of flare-like eruptions, and found that the profiles of intersystem lines were frequently different from the profiles of the allowed lines.

An example is given by the Si III, O IV and Si IV lines in the spectra of the 15 June 1973 flare recorded by the NRL spectrograph on *Skylab* (Figure 11). The profiles are shown at different times. Note that around 14^h12^m a blueshifted component is present in the profile of the allowed Si IV line, but is absent in the profiles of the intersystem Si III and O IV lines. (The arrows indicate the shifted and unshifted component of the Si IV lines.) One reason for these differences is that a profile may frequently represent a composite of different emitting regions. Each of these regions may be characterized by a unique density, nonthermal motion, and net bulk motion along the line of sight (which produces a Doppler shifted profile). Then, because the intensity ratio of an intersystem to an allowed line depends on density, the profiles of intersystem lines may differ substantially from the profiles of allowed lines. In order to analyze a particular plasma in terms of a physical model using spectroscopic techniques, it is necessary to be able to determine the contributions of the different emitting regions to the total line intensities. It is only by obtaining spectral line profiles that his is possible.

Another example is shown in Figure 12, where the Doppler shifted components have been deconvolved from the unshifted profiles using a two-gaussian approximation (Doschek and Feldman, 1978). The crosses (×) show the fits to the data. It is clear that without profile information, the relative line intensities would be physically meaningless because contributions to the total line intensities arise from different regions that are physically unrelated, and the relative strengths of the different contributions depend on the type of spectral line, i.e., allowed or intersystem.

It is possible, particularly during flares, that some coronal lines such as Mg IX (368 Å, $2s^2\ ^1S_0 - 2s2p\ ^1P_1$) will be broadened by opacity, in addition to the nonthermal broadening discussed above. The study of resonance scattering of coronal lines can also give valuable information on the physical structure of the emitting regions. As mentioned, densities at million degree temperatures in flares can be greater than 10^{11} cm^{-3}. At these densities even a small path length L can give rise to an appreciable opacity τ_0 at line center. The degree of broadening can be

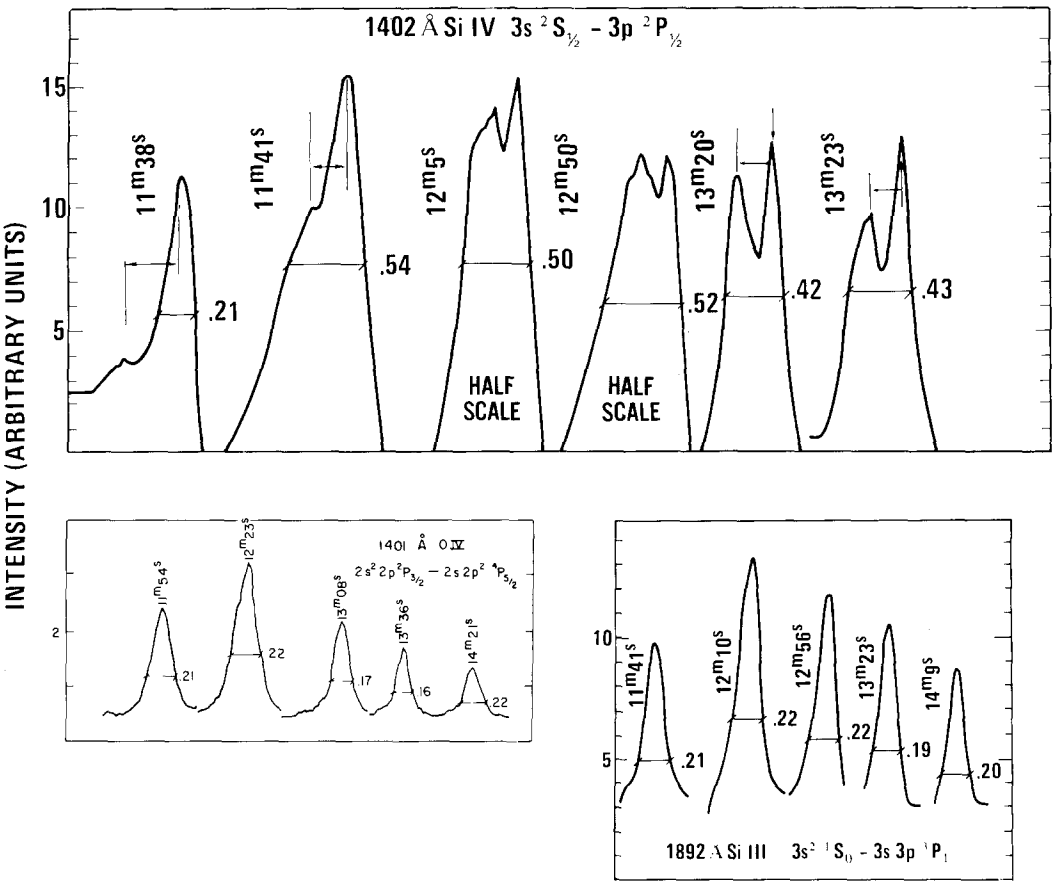

Fig. 11. Profiles of an allowed line of Si IV compared to profiles of intersystem lines of O IV and Si III for the 15 June 1973 flare observed from *Skylab*. A blue-shifted component is apparent in the Si IV line but is absent in the intersystem lines. (See Doschek *et al.*, 1977b).

approximately estimated by assuming a constant source function, which leads to an intensity distribution given by,

$$I(\lambda) \sim 1 - \exp\{-\tau_0 \exp[-(\lambda - \lambda_0)^2/\Delta\lambda_D^2]\}, \tag{12}$$

where $\Delta\lambda_D = \text{FWHM}/2\sqrt{\ln 2}$ (where the FWHM is the calculated width assuming thermal and nonthermal broadening, i.e., the values in Figure 7), and τ_0 is given by,

$$\tau_0 = \frac{\sqrt{\pi}\, e^2}{mc^2} \frac{f\lambda^2}{\Delta\lambda_D} N_g L, \tag{13}$$

where f is the absorption oscillator strength, e is the electronic charge, m is the electron mass, and N_g is the ground state density of the ion in question. Consider Mg IX as an example. For $N_e = 5 \times 10^{11}$ cm^{-3}, $\tau_0 = 1$ for $L = 440$ km, a small distance for coronal-type phenomena. Thus, a feature at a density of 5×10^{11} cm^{-3} and

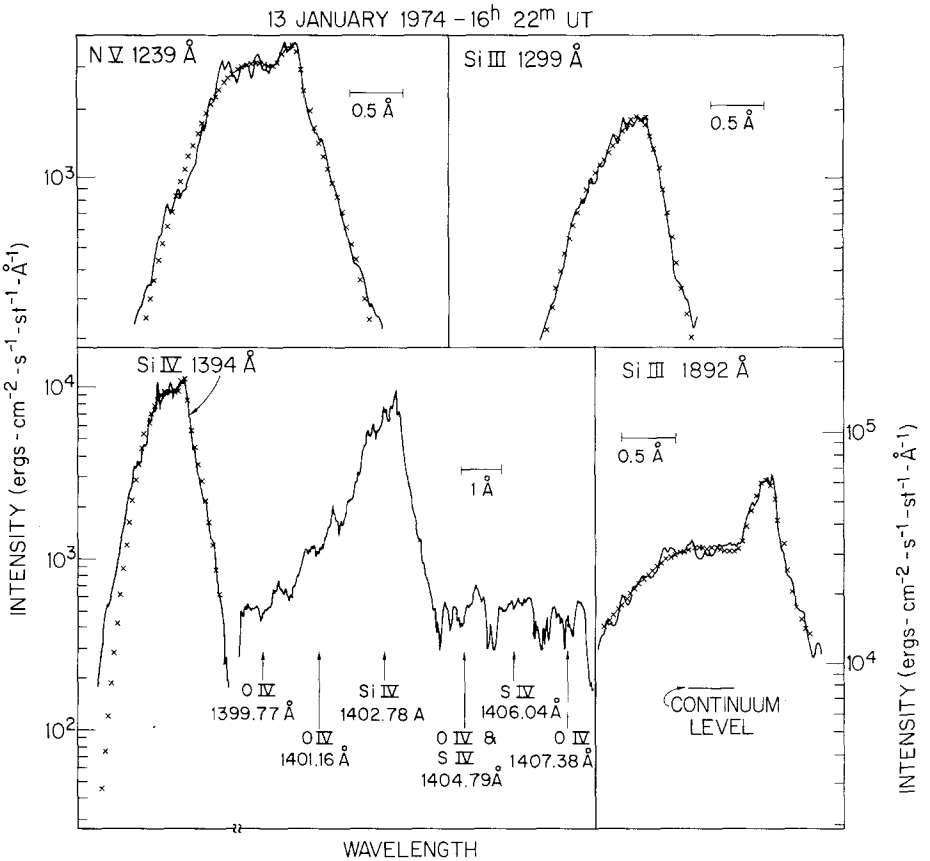

Fig. 12. Spectral line profiles of a spray or surge event recorded by the NRL spectrograph on *Skylab*. A wide blueshifted component is apparent. The crosses correspond to a two-gaussian fit to the data. (See Doschek and Feldman, 1978.)

roughly only 3″ in size (≈2300 km, the spatial resolving power of the NRL spectroheliograph flown on Skylab) would give rise to an opacity of about 5 in the Mg IX line. From Equation (12) the observed FWHM would be about 0.10 Å, instead of 0.059 Å, the width of an optically thin line. The same result would be obtained for $L \approx 100$ km and $N_e \approx 10^{13}$ cm^{-3}. Such high densities may occur in solar flares, and thus knowledge of the broadening due to opacity and the density (obtained from line ratios) enables a characteristic path length to be determined.

6. A Spectrograph for the Grazing Incidence Region

We consider in this section the characteristics of a spectrograph that would enable the measurements discussed in the previous section to be carried out. Such an instrument must have high spectral resolution, and also high spatial resolution in order to specify as well as possible the geometry of the emitting structure or

structures. A spectrograph with the necessary instrumental characteristics is shown in Figure 13. The instrumental parameters are given in Tables VI and VII.

The two cylindrical mirrors in Figure 13 are used to collect light and provide spatial resolution. Mirror II selects a narrow rectangular segment of the solar disk and focuses the light in this segment onto the slit. This light is diffracted and focussed by a concave spherical grating onto the film plane and produces an astigmatic image, i.e., no spatial resolution. The purpose of mirror I is to focus the light, collected by mirror II, onto the film plane. Thus the combination of mirror I and mirror II produces a stigmatic image at the film plane. The net result is a spectral line with spatial resolution along the length of it.

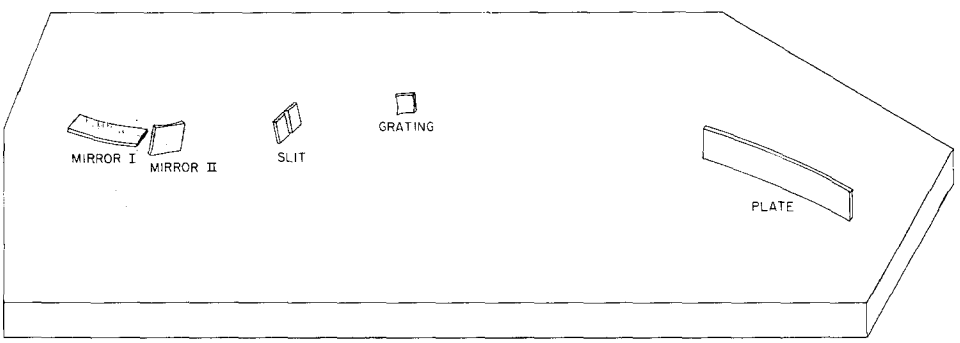

Fig. 13. Simplified layout of a high spectral resolution grazing incidence spectrograph for observation of the solar spectrum.

TABLE VI

Mirror parameters

	Mirror I	Mirror II
Focal length (f)	$\approx$1700 mm	$\approx$300 mm
f-number	2×10^{-2}	3×10^{-2}
Angle of incidence	75°	$\approx$81°
Illuminated length	$\approx$100 mm	
Illuminated width	$\approx$10 mm	

TABLE VII

Spectrograph parameters

Grating:	spherical, gold coated, 3 m radius of curvature, 1200 lines mm^{-1}, 8.4° blaze angle
Angle of incidence:	86°
Illuminated width:	$\approx$30 mm
Slit width:	4 μm
Spectral resolution:	$\Delta\lambda \approx 0.025$ Å at 600 Å $\Delta\lambda \approx 0.01$ Å at 200 Å

However, because the optical components are operating in grazing, and not normal incidence, mirror I will provide a well focussed image at only one point along the film plane. Lines that fall to either side of this point will become more and more astigmatic, the further away they are from the focal point. Thus, it is highly desirable that mirror I be moveable. By increasing or decreasing the distance of mirror I from the slit, the focal point of mirror I can be moved along the film plane. In practice, then, any particular spectral line of interest can be made stigmatic.

The characteristics of the mirrors are given in Table VI. The spectrograph parameters are given in Table VII. It can be seen that the spectral resolution is quite high, 0.01 Å at 200 Å and 0.025 Å at 600 Å. This instrument is an improved version of a 3 m grazing incidence spectrograph that has already been built and successfully flown. The spectrograph is described by Behring *et al.* (1973).

Acknowledgements

We thank Dr H. Zirin for suggesting that we review the diagnostic potential of the 80–800 Å region for solar physics. We thank Drs A. K. Bhatia, D. Flower, and H. E. Mason for sending us atomic data in advance of publication.

References

Aller, L. H., Ufford, C. W., and Van Vleck, J. H.: 1949, *Astrophys. J. Letters* **109**, 42.
Bhatia, A. K.: 1978, private communication.
Bhatia, A. K. and Mason, H. E.: 1978, *Monthly Notices Roy. Astron. Soc.* **184**, 423.
Bhatia, A. K. and Mason, H. E.: 1979, preprint.
Behring, W. E., Cohen, L., and Feldman, U.: 1972, *Astrophys. J.* **175**, 493.
Behring, W. E., Ugiansky, R. J., and Feldman, U.: 1973, *Appl. Opt.* **12**, 528.
Behring, W. E., Cohen, L., Feldman, U., and Doschek, G. A.: 1976, *Astrophys. J.* **203**, 521.
Bely, O. and Blaha, M.: 1968, *Solar Phys.* **3**, 563.
Blaha, M.: 1971, *Solar Phys.* **17**, 99.
Boland, B. C., Dyer, E. P., Firth, J. G., Gabriel, A. H., Jones, B. B., Jordan, C., McWhirter, R. W. P., Monk, P., and Turner, R. F.: 1975, *Monthly Notices Roy. Astron. Soc.* **171**, 697.
Cheng, C.-C., Doschek, G. A., and Feldman, U.: 1978, *Astrophys. J.*, in press.
Cushman, G., Farwell, L., Codden, G., and Rense, W. A.: 1975, *J. Geophys. Res.* **80**, 482.
Dere, K. P.: 1978, *Astrophys. J.* **221**, 1062.
Dere, K. P., Horan, D. M., and Kreplin, R. W.: 1977, *Astrophys. J.* **217**, 976.
Dere, K. P., Mason, H. E., Widing, K. G., and Bhatia, A. K.: 1978, submitted to the *Astrophys. J.*
Doschek, G. A. and Feldman, U.: 1978, *Astron. Astrophys.* **69**, 11.
Doschek, G. A., Behring, W. E., and Feldman, U.: 1974, *Astrophy. J. Letters* **190**, L141.
Doschek, G. A., Feldman, U., Dere, K. P., Sandlin, G. D., VanHoosier, M. E., Brueckner, G. E., Purcell, J. D., and Tousey, R.: 1975 *Astrophys. J. Letters* **196**, L83.
Doschek, G. A., Feldman, U., and Dere, K. P.: 1977a, *Astron. Astrophys.* **60**, L11.
Doschek, G. A., Feldman, U., and Rosenberg, F. D.: 1977b, *Astrophys. J.* **215**, 329.
Fawcett, B. C. and Cowan, R. D.: 1975, *Monthly Notices Roy. Astron. Soc.* **171**, 1.
Feldman, U.: 1976, *Astrophys. Space Sci.* **41**, 155.
Feldman, U. and Behring, W. E.: 1974, *Astrophys. J. Letters* **189**, L45.
Feldman, U., Doschek, G. A., and Rosenberg, F. D.: 1977, *Astrophys. J.* **215**, 652.
Feldman, U., Doschek, G. A., Mariska, J. T., Bhatia, A. K., and Mason, H. E.: 1978a, *Astrophys. J.*, in press.

Feldman, U., Doschek, G. A., and Widing, K. G.: 1978b, *Astrophys. J.* **219**, 304.
Flower, D. R.: 1977a, *Astron. Astrophys.* **56**, 451.
Flower, D. R.: 1977b, *Astron. Astrophys.* **54**, 163.
Flower, D. R.: 1978, private communication.
Flower, D. R. and Nussbaumer, H.: 1974, *Astron. Astrophys.* **31**, 353.
Gabriel, A. H. and Jordan, C.: 1972, in E. W. McDaniel and M. R. C. McDowell (eds.), *Case Studies in Atomic Collision Physics*, Vol. 2, North-Holland Publ. Co., Amsterdam.
Jordan, C.: 1969, *Monthly Notices Roy. Astron. Soc.* **142**, 501.
Kastner, S. O., Neupert, W. M., and Swartz, M.: 1974, *Astrophys. J.* **191**, 261.
Kononov, E. Ya., Koshelev, K. N., Podobedova, L. I., and Churilov, S. S.: 1975, *Soviet Opt. Spectrosc.* **39**, 458.
Kononov, E. Ya., Koshelev, K. N., Podobedova, L. I., Chakalin, S. V., and Churilov, S. S.: 1976, *J. Phys.* B **9**, 565.
Malinovsky, M. and Heroux, L.: 1973, *Astrophys. J.* **181**, 1009.
Mariska, J. T., Feldman, U., and Doschek, G. A.: 1978, *Astrophys. J.*, in press.
Mason, H. E.: 1975, *Monthly Notices Roy. Astron. Soc.* **170**, 651.
Mason, H. E.: 1978, private communication.
Mason, H. E. and Nussbaumer, H.: 1977, *Astron. Astrophys.* **54**, 547.
Mason, H. E. and Storey, P. J.: 1978, preprint.
Mason, H. E., Doschek, G. A., Feldman, U., and Bhatia, A. K.: 1978, *Astron. Astrophys.*, in press.
Nussbaumer, H.: 1976, *Astron. Astrophys.* **48**, 93.
Nussbaumer, H.: 1978, preprint.
Van Regemorter, H.: 1962, *Astrophys. J.* **136**, 906.